Enhanced Interface-Driven Perpendicular Magnetic Anisotropy by Symmetry Control in Oxide Superlattices

Di Yi, Houari Amari, Purnima P. Balakrishnan, Christoph Klewe, Alpha T. N'Diaye, Padraic Shafer, Nigel Browning, and Yuri Suzuki

Phys. Rev. Applied **15**, 024001 — Published 1 February 2021

DOI: 10.1103/PhysRevApplied.15.024001

Enhanced interface-driven perpendicular magnetic anisotropy by symmetry control in oxide superlattices

Di Yi[1,†,], Houari Amari[2,#], Purnima P. Balakrishnan[1,3,&], Christoph Klewe[4], Alpha T. N'Diaye[4], Padraic Shafer[4], Nigel Browning[2] and Yuri Suzuki[1,5]*

1 Geballe Laboratory for Advanced Materials, Stanford University, Stanford, CA, 94305, USA

2 School of Engineering and School of Physical Sciences, University of Liverpool, Liverpool, L69 3GQ, UK

3 Department of Physics, Stanford University, Stanford, CA, 94305, USA

4 Advanced Light Source, Lawrence Berkeley National Laboratory, Berkeley, CA, 94720, USA

5 Department of Applied Physics, Stanford University, Stanford, CA, 94305, USA

[†] **Current**: State Key Laboratory of New Ceramics and Fine Processing, School of Materials Science and Engineering, Tsinghua University, Beijing 100084, China

[#] **Current**: Leibniz-Institut fuer Kristallzuechtung (IKZ), Max-Born-Str. 2, 12489 Berlin, Germany

[&] **Current**: NIST Center for Neutron Research, National Institute of Standards and Technology, Gaithersburg, MD, 20899, USA

*** Email:** diyi@mail.tsinghua.edu.cn

Perpendicular magnetic anisotropy (PMA) has recently been shown to emerge at interfaces of 3*d* and 5*d* transition metal oxides (TMOs). However, strategies to systematically stabilize such interface-driven PMA still remains elusive, hindering further applications of this design approach. Here, tuning crystal symmetry is shown to be an effective means to engineer this interfacial phenomenon. The evolution of PMA strength as a function of ferromagnetic oxide thickness quantitatively reveals the competition between volume- and interface-specific contributions that determine the magnetic anisotropy. By applying different degrees of epitaxial strain, the relative contributions to PMA are modulated, clearly revealing their correlations with crystal symmetries. To be more specific, the volume anisotropy energy is found to be correlated

with the tetragonal distortion of the ferromagnetic layer, while the interface anisotropy energy is mainly modulated by the octahedral tilting at the interface. With these insights, superlattices with enhanced interface-driven PMA and higher Curie temperature are realized. These findings reveal a route to engineering interface-driven PMA and associated magnetic phenomena in TMOs heterostructures for future spintronic applications.

□. Introduction

Ferromagnetic thin films that show perpendicular magnetic anisotropy (PMA), where the magnetic moments preferentially point perpendicular to the film plane, have been of both fundamental and technological interests [1]. Due to demagnetization effects, ferromagnetic thin films tend to exhibit magnetic moments pointing in the plane of the film and thereby an in-plane magnetic anisotropy. Extensive research effort has been devoted to finding ways to overcome this in-plane magnetic anisotropy and to stabilize PMA.

Transition metal oxides (TMOs) comprise a promising family of magnetic materials with regard to the strong interplay of spin, charge, orbital and lattice degrees of freedom [2-4]. Recent research efforts have been devoted to exploring chiral magnetic structures in oxides heterostructures, governed by the delicate balance between PMA and other energy contributions [5,6]. So far, most studies have been focused on $SrRuO_3$ [7-12] but its low Curie temperature (T_c ~ 150 K) motivates the need to identify and tune PMA in other oxides. Previous studies have shown that tuning tetragonal distortion can change the strength of PMA [13-16]. However, this approach is limited in that large tetragonal distortions could suppress ferromagnetic coupling in many TMOs. For instance, in ferromagnetic $La_{0.7}Sr_{0.3}MnO_3$ (LSMO, T_c ~ 350 K), compressive strain that is required to induce PMA also leads to the splitting of e_g orbitals. The orbital splitting suppresses ferromagnetism, especially in ultrathin films where thickness confinement becomes important [17,18]. Recent advances have shown that 3*d*/5*d* TMOs interfaces can induce PMA even if the tetragonal distortion of the 3*d* ferromagnetic oxide favors

the in-plane easy direction [19], showing the potential to explore exotic magnetic states and spintronic applications at the nanometer scale near interfaces [20-22]. However, this interfacial PMA has so far only been shown in superlattices comprised of alternating one unit-cell $La_{1-x}Sr_xMnO_3$ and $SrIrO_3$ (SIO), leading to a low T_c [19,23,24]. While crystal distortions have been shown to affect PMA, the distortions associated with specific crystalline symmetries and their interplay in determining PMA are not well understood yet.

Here, we show that tuning the crystal symmetry provides an effective means to optimize interface-driven PMA. By systematically varying the LSMO thickness and epitaxial strain in the superlattices of LSMO and SIO, we quantitatively show that the effective uniaxial anisotropy energy along the out-of-plane direction is determined by the competition between volume (in-plane) and interface (perpendicular) contributions. Their strain dependence reveals the correlations between each contribution and the corresponding crystalline symmetry. To be more specific, the volume anisotropy energy is correlated with the anisotropy of ferromagnetic LSMO layers and can be modulated by tuning the tetragonal distortion. Moreover, strains imposed by underlying substrates also lead to different magnitudes of interface anisotropy energy, revealing the importance of local symmetry at the interface such as octahedral tilting. By tuning these structural variables, we are able to realize an enhanced interfacial PMA in superlattices with thicker LSMO and higher T_c.

□. Growth and structure characterization

Epitaxial $[(LSMO)_m(SIO)_n]_N$ superlattices, with N repeats of m (n) unit-cells of LSMO (SIO) in a period, have been grown on (001) oriented $SrTiO_3$ (STO, a_s=3.905 Å) and $(LaAlO_3)_{0.3}(Sr_2TaAlO_6)_{0.7}$ (LSAT, a_s =3.868 Å) substrates by using pulsed laser deposition (see the Supplemental Material [25]). Before growth, STO substrates were chemically etched and subsequently annealed to generate atomically flat surfaces. As-received LSAT substrates were used due to the difficulties in obtaining atomically flat surfaces [26,27]. The thickness of each oxide layer was in-situ controlled by using

reflection high-energy electron diffraction. Here, we focus on the superlattices with one unit-cell of SIO (n=1) in each period (Fig. 1(a)), as the strength of PMA decreases as n increases (see the Supplemental Material [25]). The thickness of LSMO in one period ranges from one (m=1) to ten (m=10) unit-cells. The total thickness is approximately 20 nm for all samples. We have also grown single-layer LSMO films on the two substrates as references.

Fig. 1(b) shows the scanning transmission electron microcopy (STEM) image of a representative superlattice (m=4) on STO. The result shows that one unit-cell of SIO (bright contrast due to the large atomic number of Ir) is sandwiched between four unit-cells of LSMO, consistent with the design. Fig. 1(c) shows the XRD spectra of the $[(LSMO)_m(SIO)_1]_N$ superlattices with m=1, 2 and 4 on STO (top) and LSAT (bottom). The satellite peaks corresponding to the superlattice structure and the finite-size oscillations arising from the thickness are clearly observed, showing the high degree of crystallinity and the precise control of periodicity. The superlattices on LSAT show a larger compressive strain. For instance, the c/a ratio is about 1.035 for the m =1 superlattices on LSAT and is about 1.015 for those on STO. It is noted that even the superlattice with the largest c/a ratio is still coherently strained by the underlying substrate, as shown by reciprocal space mapping. Further structural characterization is included in the Supplemental Material [25].

□. Ferromagnetism and orbital polarization

We first examined ferromagnetic properties of the $[(LSMO)_m(SIO)_1]_N$ superlattices when the thickness of LSMO is reduced from m=10 (4 nm) to m=1 (0.4 nm). Fig. 2 shows the summary of T_c and saturation magnetization M_s (where the total magnetic signal is averaged over the volume of LSMO) of the superlattices grown on STO (green) and LSAT (red). The values of T_c are determined to be the point where there is a change in curvature of the temperature dependent magnetization and M_s is obtained from the magnetic hysteresis loop at 10 K in fields of up to 7 T. The magnitudes of M_s are also confirmed by x-ray magnetic circular dichroism (XMCD) to rule out contributions from the

substrates (see the Supplemental Material [25]). As shown in Fig. 2, for superlattices with m>4, T_c is close to 300 K and M_s is approximately 450 emu cm^{-3} on both substrates. By reducing m, superlattices on LSAT show a quick deterioration of ferromagnetic properties, manifest as a fast decline of both T_c and M_s. It is noted that ferromagnetic behavior is observed for all superlattices grown on STO. The m=1 superlattices on STO exhibit T_c around 150 K and M_s about 340 emu cm^{-3}. By contrast, no clear ferromagnetic transition is observed for the m=1 superlattices on LSAT.

To gain insight into the evolution of ferromagnetic properties, we carried out x-ray linear dichroism (XLD) measurements at the Mn L-edges. The XLD measurements were performed above the Curie temperature of those superlattices. Therefore, the magnitude is proportional to the energy splitting of two e_g orbitals, i.e. $d(3z^2\text{-}r^2)$ and $d(x^2\text{-}y^2)$ [28-30]. Fig. 3 shows the XLD spectra of the superlattices with different values of m on LSAT, superlattices with m=1 on STO and reference LSMO films on LSAT. First, the magnitude of the XLD signal for the m=1 superlattices on LSAT is significantly larger than that of the LSMO films on LSAT, indicating that the orbital splitting is affected by the interfacial orbital reconstruction. This is further supported by the thickness dependence of XLD signal for the superlattices on LSAT, which decreases as m increases as shown in Fig. 3. Moreover, we observe that the magnitude of the XLD signal for the m=1 superlattices on LSAT is also larger than that of the m=1 superlattices on STO, revealing an additional contribution from the strain-induced tetragonal distortion. It is noted that the orbital splitting decreases the kinetic energy of e_g electrons and the double-exchange interactions [31]. In addition, we do not observe a clear valence change of Mn cations as revealed by the x-ray absorption spectra [32] (see the Supplemental Material [25]). Therefore, the suppression of ferromagnetism in the m=1 superlattices on LSAT is likely due to this large e_g orbital splitting.

□. Perpendicular magnetic anisotropy

Having established the ferromagnetic properties, we then studied the PMA of superlattices. Magnetic hysteresis loops were measured along both in-plane ([100]) and out-of-plane ([001]) directions for all samples except the superlattices that show very small M_s (i.e. m=1 and 2 superlattices on LSAT). First, for single-layer LSMO films, we find that the magnetic easy axis is within the film plane on both substrates (see the Supplemental Material [25]). This is expected by considering shape anisotropy and strain effect [14]. Secondly, interface-driven PMA is observed in superlattices on both substrates. Fig. 4(a) shows the hysteresis loops along out-of-plane (red) and in-plane (blue) directions for the m=3 superlattices on LSAT at 10K. The distinct differences clearly reveal the emergence of PMA. Fig. 4(b) shows the temperature dependence of magnetization, measured with a magnetic field of 0.1 T along both directions. The difference in magnetization is observed up to 200K (T_c ~ 230 K), revealing the robustness of PMA. The temperature dependence of PMA is further revealed by measuring magnetic hysteresis loops at elevated temperatures with an easy axis along the out-of-plane direction (see Fig. 4(c) and the Supplemental Material [25]).

Intriguingly, the interface-driven PMA is strongly modulated by the epitaxial strain. Fig. 4(d) and 4(e) show the hysteresis loops along both directions for the m=4 superlattices on LSAT and STO. The m=4 superlattices on LSAT still show magnetic easy axis close to the out-of-plane direction, although the strength of PMA decreases as compared to the m=3 counterparts. By contrast, the magnetic easy axis of the m=4 superlattices on STO is within the film plane, manifest as the nearly zero remnant magnetization and high saturation field along the out-of-plane direction. Results on superlattices with other m values are presented in the Supplemental Material [25]. To quantify the strength of PMA, we estimate an effective uniaxial anisotropy energy (K_u) associated with the PMA by the area enclosed between magnetization curves along the two directions [33]. By this definition, the positive (negative) K_u corresponds to the easy axis along out-of-plane (in-plane) direction and its magnitude reflects the strength of anisotropy energy. Fig. 4(f) summarizes the change of K_u as a

function of m in $[(LSMO)_m(SIO)_1]_N$ on two substrates. First, the superlattices with the same m exhibit a much stronger PMA on LSAT. It is noted that the K_u of the m=3 superlattices on LSAT ($K_u \sim 6\times10^5$ erg cm^{-3}) is already larger than that of the m=1 superlattices on STO, in which the K_u should be dominated by the interface contribution [19]. Moreover, the magnitude of K_u decreases by increasing m on both substrates, consistent with the fact that PMA is induced by the interface. We also find that the superlattices on STO exhibit a faster decay of K_u as m increases.

□. Correlation between anisotropy energy and symmetry

Phenomenologically, the effective uniaxial anisotropy energy K_u can be separated into two contributions, i.e. the volume anisotropy energy K_v (erg cm^{-3}) and the interface anisotropy energy K_s (erg cm^{-2}), which approximately follow the correlation [33-35]:

$$K_u = K_v + 2\,K_s/t \quad (1)$$

The term K_s/t represents the decay of the interface contribution in the inner region of a ferromagnetic layer, bound by two interfaces that lead to the prefactor of two. To quantitatively analyze different anisotropy contributions, we plot the uniaxial anisotropy energy times LSMO thickness in a period (K_ut) as a function of t in Fig. 5(a). The dependence of K_ut on t approximately follows the linear correlation, as shown by the solid lines in Fig. 5(a). Similar evolution of PMA with ferromagnetic layer thickness has been reported in other systems that show interface-driven PMA, including heterostructures comprised of ferromagnetic metals and 5*d* transition metals [33,34] or binary oxides [35,36] as well as heterostructures comprised of TMOs with oxygen octahedra and tetrahedra [37]. According to Equation (1), the slope of the linear function corresponds the volume anisotropy energy K_v while the intercept at zero thickness reveals the interface anisotropy energy $2K_s$. This quantitative analysis provides insights into the correlations between PMA and crystalline symmetries.

First, we find that the superlattices on two substrates show different magnitudes of volume anisotropy energy K_v. The magnitude of K_v is found to be about -1.8×10^6 erg cm^{-3} for the superlattices

on STO and about -1.0×10^6 erg cm^{-3} for those on LSAT. It is noted that the magnitudes of K_v are very close to the effective uniaxial anisotropy energies of single-layer LSMO films on corresponding substrates, which are found to be roughly -2.0×10^6 erg cm^{-3} and -1.1×10^6 erg cm^{-3} at 10 K for LSMO films on STO and LSAT (see the Supplemental Material [25]). These results suggest that the K_v is mainly correlated to the inner regions of LSMO layer in the superlattices, governed by the shape anisotropy (negative) and strain-induced anisotropy (positive for compressively strained LSMO) [13-16]. Therefore, as shown in Fig. 5(b), the magnitude of K_v, which dictates how fast PMA decays as the thickness of ferromagnetic layer increases, can be tuned by epitaxial strain that modifies the tetragonal distortion (*c/a* ratio).

Intriguingly, the superlattices on two substrates also show different magnitudes of interface anisotropy energy K_s. As revealed in Fig. 5(a), the magnitude of K_s in the superlattices on LSAT (about 0.1 erg cm^{-2}) is roughly twice as large as that of the superlattices on STO. Given that the constituent materials are identical, the difference in K_s should arise from the local symmetry at the interface, which affects the coupling between Ir and Mn cations. Our previous study has shown that the strength of PMA in the m=1 superlattice is mainly correlated with the octahedral tilting across the interface and that straight Ir-O-Mn bonds lead to a strong PMA [19]. It is noted that the results here are consistent with this conclusion. It has been shown both theoretically and experimentally that an increase in compressive strain will suppress the octahedral tilting (rotation along the in-plane [100] direction, Fig. 5(b)) [38-41]. Therefore, the magnitude of octahedral tilting (ω_a) decreases in superlattices on LSAT as compared to the counterparts on STO [42], leading to straight bonds (larger θ) and therefore an enhancement of K_s. It is noted that the interfacial layers of superlattices on LSAT would also show a larger tetragonal distortion, which might contribute to the enhancement of K_s [43,44]. As demonstrated in our previous results, octahedral tilting appears to play the dominant role in determining the strength of PMA induced at this 3*d*/5*d* interface [19].

The correlations between different contributions to PMA and corresponding crystalline symmetries (Fig. 5(b)) provide a useful guide to design oxides heterostructures with PMA and associated emergent magnetic phenomena. First, to sustain PMA in thicker ferromagnetic oxide with higher T_c, one should tune the oxide for an optimal *c/a* ratio that can enhance K_v without suppressing ferromagnetic exchange coupling. This is exemplified by the *m*=3 superlattices on LSAT that show PMA up to 200 K (Fig. 4(b)), much higher than that of the *m*=1 superlattices on STO in previous reports [19]. Moreover, the strength of K_s is correlated with the octahedral tilting; therefore oxides with a cubic structure, and without tilting, might enhance K_s. Taking all of this into account, it is worthwhile to study ferromagnetic manganates that have a large lattice constant and a cubic structure, such as $La_{1-x}Ba_xMnO_3$ [45,46], in heterostructures with 5*d* TMOs. Furthermore, strain-tunable anisotropy energies suggest that piezoelectric oxides may be integrated to realize the active control of exotic magnetic states [47,48].

□. Conclusion

In conclusion, we have systematically studied the interface-driven PMA in 3*d*/5*d* TMOs heterostructures as a function of ferromagnetic layer thickness and epitaxial strain. Our data show that the emergent PMA is determined by the competition between volume- and interface-specific contributions in the superlattices. More importantly, the correlations between the two contributions and the corresponding crystalline symmetries have been established. The volume contribution is mainly correlated with the tetragonal distortion of the ferromagnetic oxide. The interface contribution is found to be governed by octahedral tilting. By optimizing these energy contributions, we are able to realize superlattices with improved performances. Our results provide strategies for engineering correlated oxides heterostructures with emergent magnetic phenomena in potential memory applications.

Acknowledgments

The work at Stanford was supported by the Air Force Office of Scientific Research under Grant FA9550-16-1-0235 and FA9550-20-1-0293. P.P.B. was supported by the National Science Foundation under Grant No. 1762971. This research used resources of the Advanced Light Source, which is a DOE Office of Science User Facility under Contract No. DE-AC02-05CH11231. Part of this work was performed at the Stanford Nano Shared Facilities (SNSF), supported by the National Science Foundation under award ECCS-1542152.

References

[1] S. Bhatti, R. Sbiaa, A. Hirohata, H. Ohno, S. Fukami, and S. N. Piramanayagam, Spintronics based random access memory: a review, Mater. Today **20**, 530 (2017).

[2] P. Zubko, S. Gariglio, M. Gabay, P. Ghosez, and J. M. Triscone, in *Annual Review of Condensed Matter Physics, Vol 2*, edited by J. S. Langer (Annual Reviews, Palo Alto, 2011), pp. 141.

[3] H. Y. Hwang, Y. Iwasa, M. Kawasaki, B. Keimer, N. Nagaosa, and Y. Tokura, Emergent phenomena at oxide interfaces, Nat. Mater. **11**, 103 (2012).

[4] A. Bhattacharya and S. J. May, in *Annual Review of Materials Research, Vol 44*, edited by D. R. Clarke (Annual Reviews, Palo Alto, 2014), pp. 65.

[5] A. Fert, N. Reyren, and V. Cros, Magnetic skyrmions: advances in physics and potential applications, Nat. Rev. Mater. **2**, 15 (2017).

[6] W. J. Jiang, G. Chen, K. Liu, J. D. Zang, S. G. E. te Velthuis, and A. Hoffmann, Skyrmions in magnetic multilayers, Phys. Rep.-Rev. Sec. Phys. Lett. **704**, 1 (2017).

[7] J. Matsuno, N. Ogawa, K. Yasuda, F. Kagawa, W. Koshibae, N. Nagaosa, Y. Tokura, and M. Kawasaki, Interface-driven topological Hall effect in $SrRuO_3$-$SrIrO_3$ bilayer, Sci. Adv. **2**, 7, UNSP e1600304 (2016).

[8] L. F. Wang, Q. Y. Feng, Y. Kim, R. Kim, K. H. Lee, S. D. Pollard, Y. J. Shin, W. Peng, D. Lee, W. J. Meng *et al.*, Ferroelectrically tunable magnetic skyrmions in ultrathin oxide heterostructures, Nat. Mater. **17**, 1087 (2018).

[9] Q. Qin, L. Liu, W. N. Lin, X. Y. Shu, Q. D. Xie, Z. Lim, C. J. Li, S. K. He, G. M. Chow and J. S. Chen,., Emergence of Topological Hall Effect in a $SrRuO_3$ Single Layer, Adv. Mater. **31**, 6, 1807008 (2019).

[10] K. Y. Meng, A. S. Ahmed, M. Bacani, A. O. Mandru, X. Zhao, N. Bagues, B. D. Esser, J. Flores, D. W. McComb, H. J. Hug and F. Y. Yang, Observation of Nanoscale Skyrmions in $SrIrO_3/SrRuO_3$ Bilayers, Nano Lett. **19**, 3169 (2019).

[11] W. B. Wang, M. W. Daniels, Z. L. Liao, Y. F. Zhao, J. Wang, G. Koster, G. Rijnders, C. Z. Chang, D. Xiao and W. D. Wu, Spin chirality fluctuation in two-dimensional ferromagnets with perpendicular magnetic anisotropy, Nat. Mater. **18**, 1054 (2019).

[12] Y. D. Gu, Y. W. Wei, K. Xu, H. R. Zhang, F. Wan, F. Li, M. S. Saleem, C. Z. Chang, J. R. Sun, C. Song *et al.*, Interfacial oxygen-octahedral-tilting-driven electrically tunable topological Hall effect in ultrathin $SrRuO_3$ films, J. Phys. D-Appl. Phys. **52**, 13, 404001 (2019).

[13] Y. Suzuki, H. Y. Hwang, S. W. Cheong, and R. B. vanDover, The role of strain in magnetic anisotropy of manganite thin films, Appl. Phys. Lett. **71**, 140 (1997).

[14] K. Steenbeck and R. Hiergeist, Magnetic anisotropy of ferromagnetic $La_{0.7}(Sr,Ca)_{0.3}MnO_3$ epitaxial films, Appl. Phys. Lett. **75**, 1778 (1999).

[15] C. H. Du, R. Adur, H. L. Wang, A. J. Hauser, F. Y. Yang, and P. C. Hammel, Control of Magnetocrystalline Anisotropy by Epitaxial Strain in Double Perovskite Sr_2FeMoO_6 Films, Phys. Rev. Lett. **110**, 5, 147204 (2013).

[16] J. Walter, S. Bose, M. Cabero, G. C. Yu, M. Greven, M. Varela, and C. Leighton, Perpendicular magnetic anisotropy via strain-engineered oxygen vacancy ordering in epitaxial $La_{1-x}Sr_xCoO_{3-\delta}$, Phys. Rev. Mater. **2**, 8, 111404 (2018).

[17] A. Tebano, C. Aruta, P. G. Medaglia, F. Tozzi, G. Balestrino, A. A. Sidorenko, G. Allodi, R. De Renzi, G. Ghiringhelli, C. Dallera *et al.*, Strain-induced phase separation in $La_{0.7}Sr_{0.3}MnO_3$ thin films, Phys. Rev. B **74**, 7, 245116 (2006).

[18] C. Aruta, G. Ghiringhelli, A. Tebano, N. G. Boggio, N. B. Brookes, P. G. Medaglia, and G. Balestrino, Strain induced x-ray absorption linear dichroism in $La_{0.7}Sr_{0.3}MnO_3$ thin films, Phys. Rev. B **73**, 8, 235121 (2006).

[19] D. Yi, C. L. Flint, P. P. Balakrishnan, K. Mahalingam, B. Urwin, A. Vailionis, A. T. N'Diaye, P. Shafer, E. Arenholz, Y. Choi *et al.*, Tuning Perpendicular Magnetic Anisotropy by Oxygen Octahedral Rotations in $(La_{1-x}Sr_xMnO_3)/(SrIrO_3)$ Superlattices, Phys. Rev. Lett. **119**, 6, 077201 (2017).

[20] L. Liu, Q. Qin, W. N. Lin, C. J. Li, Q. D. Xie, S. K. He, X. Y. Shu, C. H. Zhou, Z. Lim, J. H. Yu *et al.*, Current-induced magnetization switching in all-oxide heterostructures, Nat. Nanotechnol. **14**, 939 (2019).

[21] S. Crossley, A. G. Swartz, K. Nishio, Y. Hikita, and H. Y. Hwang, All-oxide ferromagnetic resonance and spin pumping with $SrIrO_3$, Phys. Rev. B **100**, 7, 115163 (2019).

[22] T. Nan, T. J. Anderson, J. Gibbons, K. Hwang, N. Campbell, H. Zhou, Y. Q. Dong, G. Y. Kim, D. F. Shao, T. R. Paudel *et al.*, Anisotropic spin-orbit torque generation in epitaxial SrIrO3 by symmetry design, Proc. Natl. Acad. Sci. U. S. A. **116**, 16186 (2019).

[23] D. Yi, J. Liu, S. L. Hsu, L. P. Zhang, Y. Choi, J. W. Kim, Z. H. Chen, J. D. Clarkson, C. R. Serrao, E. Arenholz *et al.*, Atomic-scale control of magnetic anisotropy via novel spin-orbit coupling effect in $La_{2/3}Sr_{1/3}MnO_3/SrIrO_3$ superlattices, Proc. Natl. Acad. Sci. U. S. A. **113**, 6397 (2016).

[24] J. Nichols, X. Gao, S. Lee, T. L. Meyer, J. W. Freeland, V. Lauter, D. Yi, J. Liu, D. Haskel, J. R. Petrie *et al.*, Emerging magnetism and anomalous Hall effect in iridate-manganite heterostructures, Nat. Commun. **7**, 6, 12721 (2016).

[25] See Supplemental Material at [URL will be inserted by publisher] for for experimental methods, additional structure, magnetic and x-ray dichroism characterizations of superlattices and reference films.

[26] J. H. Ngai, T. C. Schwendemann, A. E. Walker, Y. Segal, F. J. Walker, E. I. Altman, and C. H. Ahn, Achieving A-Site Termination on $La_{0.18}Sr_{0.82}Al_{0.59}Ta_{0.41}O_3$ Substrates, Adv. Mater. **22**, 2945 (2010).

[27] A. Biswas, C.-H. Yang, R. Ramesh, and Y. H. Jeong, Atomically flat single terminated oxide substrate surfaces, Progress in Surface Science **92**, 117 (2017).

[28] C. Aruta, G. Ghiringhelli, A. Tebano, N. G. Boggio, N. B. Brookes, P. G. Medaglia, and G. Balestrino, Strain induced x-ray absorption linear dichroism in $La_{0.7}Sr_{0.3}MnO_3$ thin films, Phys. Rev. B **73**, 8, 235121 (2006).

[29] A. Tebano, C. Aruta, S. Sanna, P. G. Medaglia, G. Balestrino, A. A. Sidorenko, R. De Renzi, G. Ghiringhelli, L. Braicovich, V. Bisogni and N. B. Brookes, Evidence of orbital reconstruction at interfaces in ultrathin $La_{0.67}Sr_{0.33}MnO_3$ films, Phys. Rev. Lett. **100**, 4, 137401 (2008).

[30] D. Pesquera, G. Herranz, A. Barla, E. Pellegrin, F. Bondino, E. Magnano, F. Sanchez, and J. Fontcuberta, Surface symmetry-breaking and strain effects on orbital occupancy in transition metal perovskite epitaxial films, Nat. Commun. **3**, 7, 1189 (2012).

[31] Y. Tokura, Critical features of colossal magnetoresistive manganites, Rep. Prog. Phys. **69**, 797 (2006).

[32] M. Varela, M. P. Oxley, W. Luo, J. Tao, M. Watanabe, A. R. Lupini, S. T. Pantelides, and S. J. Pennycook, Atomic-Resolution Imaging of Oxidation States in Manganites, Phys. Rev. B **79**, 085117 (2009).

[33] M. T. Johnson, P. J. H. Bloemen, F. J. A. denBroeder, and J. J. deVries, Magnetic anisotropy in metallic multilayers, Rep. Prog. Phys. **59**, 1409 (1996).

[34] I. K. Schuller, S. Kim, and C. Leighton, Magnetic superlattices and multilayers, J. Magn. Magn. Mater. **200**, 571 (1999).

[35] B. Dieny and M. Chshiev, Perpendicular magnetic anisotropy at transition metal/oxide interfaces and applications, Rev. Mod. Phys. **89**, 54, 025008 (2017).

[36] S. Miwa, M. Suzuki, M. Tsujikawa, T. Nozaki, T. Nakamura, M. Shirai, S. Yuasa, and Y. Suzuki, Perpendicular magnetic anisotropy and its electric-field-induced change at metal-dielectric interfaces, J. Phys. D-Appl. Phys. **52**, 22, 063001 (2019).

[37] J. Zhang, Z. C. Zhong, X. X. Guan, X. Shen, J. N. Zhang, F. R. Han, H. Zhang, H. R. Zhang, X. Yan, Q. H. Zhang *et al.*, Symmetry mismatch-driven perpendicular magnetic anisotropy for perovskite/brownmillerite heterostructures, Nat. Commun. **9**, 9, 1923 (2018).

[38] J. M. Rondinelli, S. J. May, and J. W. Freeland, Control of octahedral connectivity in perovskite oxide heterostructures: An emerging route to multifunctional materials discovery, MRS Bull. **37**, 261 (2012).

[39] S. J. May, J. W. Kim, J. M. Rondinelli, E. Karapetrova, N. A. Spaldin, A. Bhattacharya, and P. J. Ryan, Quantifying octahedral rotations in strained perovskite oxide films, Phys. Rev. B **82**, 7, 014110 (2010).

[40] A. Vailionis, H. Boschker, W. Siemons, E. P. Houwman, D. H. A. Blank, G. Rijnders, and G. Koster, Misfit strain accommodation in epitaxial ABO_3 perovskites: Lattice rotations and lattice modulations, Phys. Rev. B **83**, 064101 (2011).

[41] B. Kim, B. H. Kim, K. Kim, and B. I. Min, Substrate-tuning of correlated spin-orbit oxides revealed by optical conductivity calculations, Scientific Reports **6**, 27095 (2016).

[42] T. R. Dasa, L. Hao, J. Y. Yang, J. Liu, and H. X. Xu, Strain effects on structural and magnetic properties of $SrIrO_3/SrTiO_3$ superlattice, Mater. Today Phys. **4**, 43 (2018).

[43] G. Jackeli and G. Khaliullin, Mott Insulators in the Strong Spin-Orbit Coupling Limit: From Heisenberg to a Quantum Compass and Kitaev Models, Phys. Rev. Lett. **102**, 017205 (2009).

[44] P. Liu, S. Khmelevskyi, B. Kim, M. Marsman, D. Li, X.-Q. Chen, D. D. Sarma, G. Kresse, and C. Franchini, Anisotropic magnetic couplings and structure-driven canted to collinear transitions in Sr_2IrO_4 by magnetically constrained noncollinear DFT, Phys. Rev. B **92**, 054428 (2015).

[45] B. Dabrowski, K. Rogacki, X. Xiong, P. W. Klamut, R. Dybzinski, J. Shaffer, and J. D. Jorgensen, Synthesis and properties of the vacancy-free $La_{1-x}Ba_xMnO_3$, Phys. Rev. B **58**, 2716 (1998).

[46] J. Zhang, H. Tanaka, T. Kanki, J. H. Choi, and T. Kawai, Strain effect and the phase diagram of $La_{1-x}Ba_xMnO_3$ thin films, Phys. Rev. B **64**, 7, 184404 (2001).

[47] Y. Wang, L. Wang, J. Xia, Z. Lai, G. Tian, X. Zhang, Z. Hou, X. Gao, W. Mi, C. Feng et al., Electric-field-driven non-volatile multi-state switching of individual skyrmions in a multiferroic heterostructure, Nat. Commun. 11, 8, 3577 (2020).

[48] H. Zhang, L. Hao, J. Y. Yang, J. Mutch, Z. Y. Liu, Q. Huang, K. Noordhoek, A. F. May, J. H. Chu, J. W. Kim *et al.*, Comprehensive electrical control of metamagnetic transition of a quasi-2D antiferromagnet by in situ anisotropic strain, Adv. Mater. **32**, 6, 2002451 (2020).

Figures

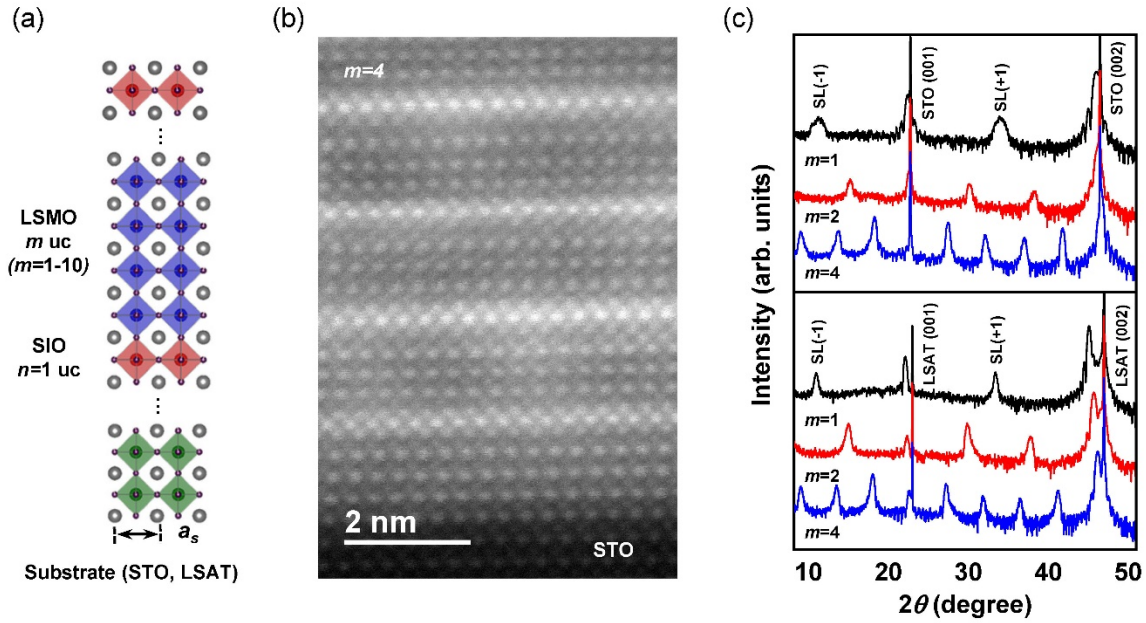

Figure 1 (a) Schematic of $[(LSMO)_m(SIO)_n]_N$ superlattices (SLs) on STO and LSAT substrates. (b) High-angle annular dark-field (HAADF) scanning transmission electron microscopy (STEM) image of a $[(LSMO)_4(SIO)_1]_{10}$ on STO. Ir cations show the brightest contrast. (c) Representative θ-2θ x-ray diffraction spectra of the SLs with different LSMO thickness (m) on STO (top) and LSAT (bottom).

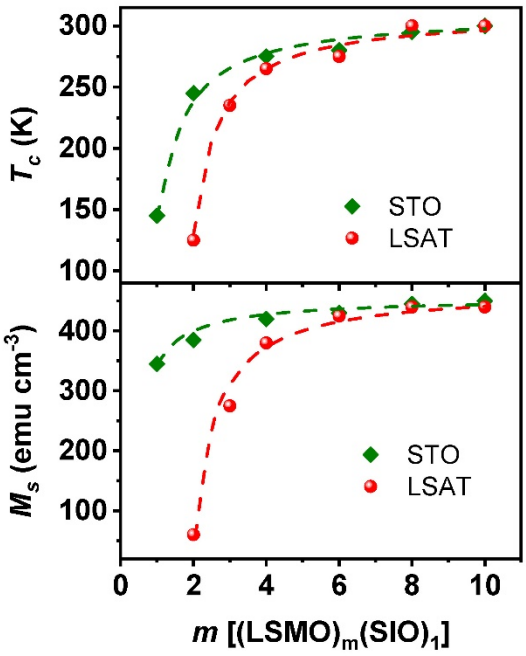

Figure 2 Ferromagnetic Curie temperature (T_c, top) and saturation magnetization (M_s, bottom) as a function of LSMO thickness (m) for the $[(LSMO)_m(SIO)_1]_N$ superlattices on STO (green) and LSAT (red) substrates.

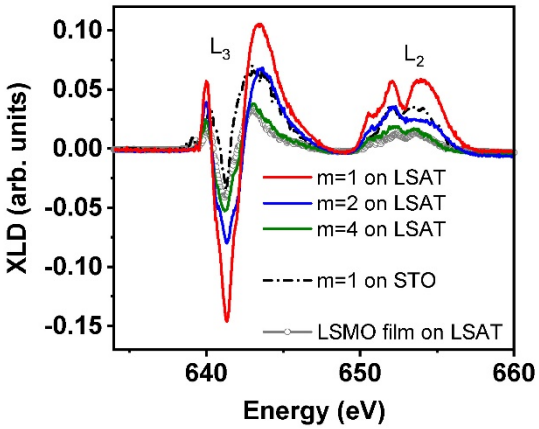

Figure 3 X-ray linear dichroism (XLD) spectra of $[(LSMO)_m(SIO)_1]_N$ superlattices on LSAT with *m*=1 (red), *m*=2 (blue) and *m*=4 (green), superlattices on STO with *m*=1 (black) and LSMO films on LSAT (grey). These spectra were measured at 300K.

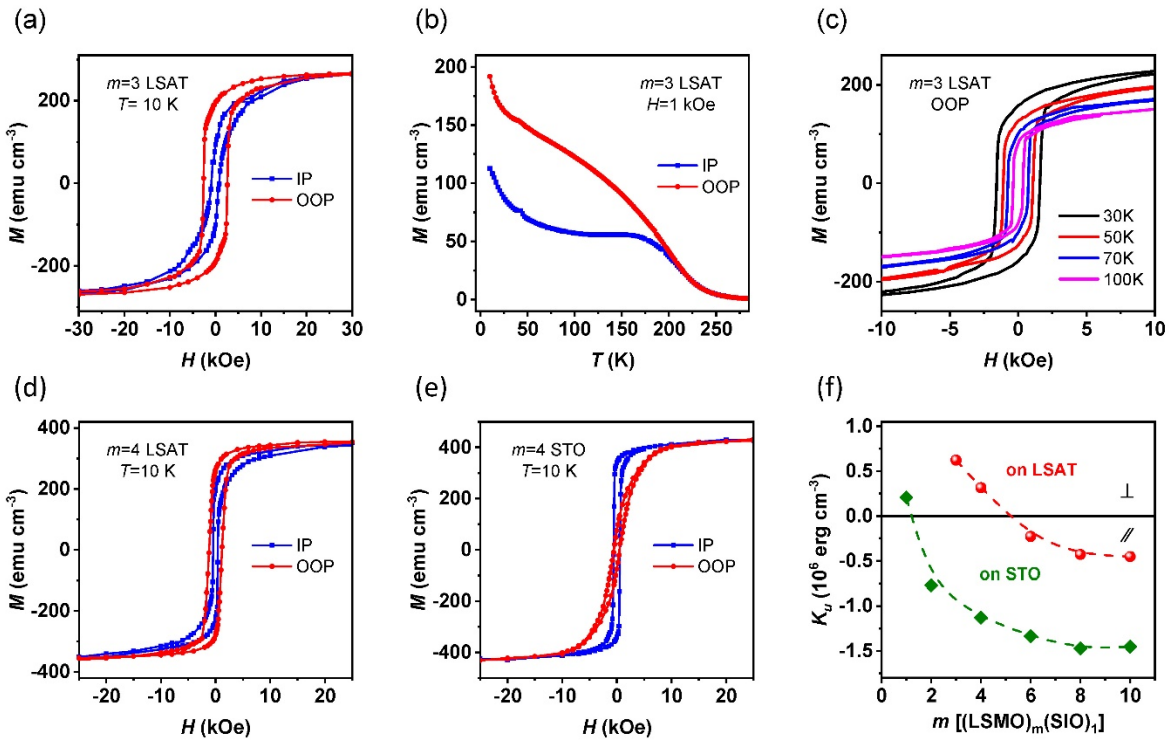

Figure 4 (a) Magnetic hysteresis loops at 10 K and (b) temperature dependence of magnetization along in-plane (IP [100]) and out-of-plane (OOP [001]) directions of an m=3 superlattice (SL) on LSAT. (c) Magnetic hysteresis loops along OOP direction (m=3) at different temperatures. (d)-(e) Magnetic hysteresis loops of SLs with m=4 on (d) LSAT and (e) STO. (f) Evolution of uniaxial magnetic anisotropy energy (K_u) as a function of LSMO thickness (m) on the two substrates.

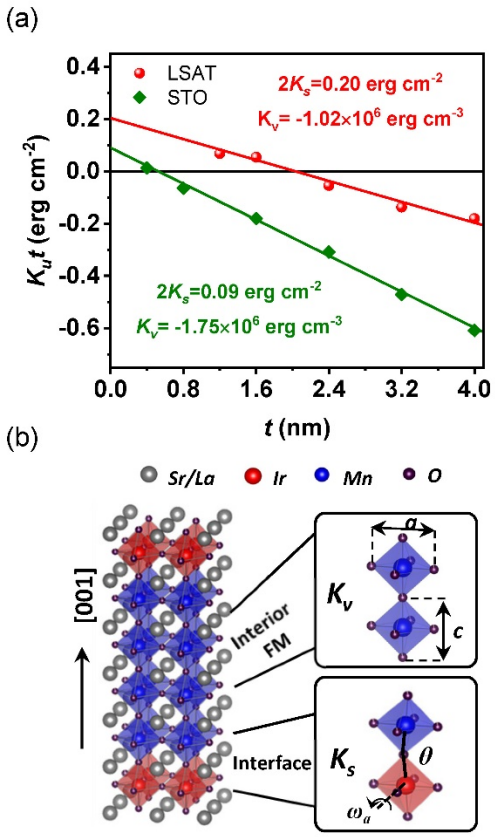

Figure 5 (a) Uniaxial magnetic anisotropy energy (K_u) times the LSMO thickness (t) versus t for the superlattices on two substrates at 10 K. The solid lines show the linear fitting by using the formula $K_u t = K_v t + 2K_s$, where K_v and K_s refer to the volume and interface anisotropy energy. (b) Schematic of correlation between the two anisotropy energies (K_v and K_s) and the corresponding crystalline symmetries (tetragonal distortion and octahedral tilting).